



Unfolding the role of topology-driven toughening mechanisms in nacre-like composite design through XFEM

Andres E. Aguilar Coello^{a,1}, Andre E. Vellwock^{b,2}, Andrea Avanzini^c, Flavia Libonati^{d,*}

^a Department of Mechanical Engineering, Politecnico di Milano, Milano, Italy

^b Department of Mechanical Engineering, The Hong Kong Polytechnic University, Hung Hom, Kowloon, Hong Kong Special Administrative Region

^c Department of Mechanical and Industrial Engineering, University of Brescia, Brescia, Italy

^d Department of Mechanical, Energy, Management and Transportation Engineering, University of Genoa, Genoa, Italy

ARTICLE INFO

Keywords:

Fracture
XFEM
Hyperelasticity
Mineral bridges
Bioinspired composites

ABSTRACT

Biological materials have evolved through thousands of years, adapting, morphing, and optimizing to their particular function. One of the many natural materials that are widely studied is nacre, an elegant merge of stiff (mineral) and soft (biopolymer) components with extremely high mechanical properties, which are highly desired for structural applications. Naturally, nacre has been a source of inspiration for developing artificial composites with different levels of intrinsic designs. Some of these designs exploit the microstructures of the materials, such as the connection between the composite stiffer parts, known as mineral bridges. To develop an eXtended Finite Element Method (XFEM)-based model of a biphasic composite inspired by the nacreous brick-and-mortar morphology, initially, we evaluate the use of XFEM on single materials models, including a hyperelastic material. Then, simulation of complex bioinspired materials shows that structures mimicking mineral bridges considerably improve composites' mechanical properties such as strength and toughness. The influence of the biomimetic mineral volume fraction on the overall toughening mechanisms, particularly crack arresting, is demonstrated. Our results provide a numerical approach to simulating biphasic materials with hyperelastic components and contrasting material properties (e.g., stiff and ductile) that have potential applications in complex composite structural designs.

1. Introduction

Natural materials are in constant self-improvement towards optimization of specialized functions such as antifouling [1,2], thermal resistance [3], and aero drag reduction [4], allowing species to evolve and easier overcome environment elements and predators. The development of nacre is a specific case where shellfish is shielded through a highly complex multiscale composite. Nacre combines two constituents to achieve remarkable material properties as a typical composite. A brick-and-mortar architecture is present at the nanoscale, where brick-shaped mineral platelets are embedded in an organic-polymeric matrix [5]. Nacre is extremely strong and tough, far exceeding the properties of its monolithic components. Moreover, the low-density constituents allow it to reach an extraordinary combination of lightness and toughness. The specific microstructure creates unique multiscale toughening

mechanisms. For instance, crack deflection and arrest [6,7], mineral bridging [8–11], brick interlocking [12,13], and viscoelastic adhesive behavior of the organic biopolymer [14–16]. The interface between platelets and matrix also plays an important role [17,18]. Through controllable designs, nacreous-inspired composite materials have been shown to experimentally replicate in engineering composites similar toughening mechanisms [19–22].

Theoretical models of the nacreous microstructure are well developed [23–25], but they cannot fully describe intricate nano- and micro-scale mechanisms. In the opposite direction, numerical models have attempted to solve the issue as they provide great versatility in studying multiple physical phenomena [26,27]. Greco, Leonetti [28] developed a multiscale model that allowed the visualization of matrix cracking on nacre-like composites. Nevertheless, the solution requires complex user-input computations. Xie, Yuan [29] created a method to evaluate the

* Corresponding author.

E-mail address: flavia.libonati@unige.it (F. Libonati).

¹ Current address: Johnson & Johnson del Ecuador S.A, Quito, Ecuador.

² Current address: B CUBE - Center for Molecular Bioengineering, Technische Universität Dresden, Dresden, Germany.

dynamic modulus of nacre-like composites. Despite accurate results, it cannot simulate failure behavior. Cohesive models [30,31] showed less sophisticated yet accurate crack propagation analysis, but the proposed approach has a significant drawback: it cannot predict the crack initiation. Thus, the user selection of the crack location can alter the propagation massively.

The eXtended Finite Element Method (XFEM) is a numerical model mainly used in fracture mechanics analysis [32], with successful applications in simulating cracks in composites [33–37], natural [38–40], and bioinspired materials [41,42]. Despite convergence issues, it can simulate the crack initiation combined with its propagation, describing the material mechanical behavior until total fracture. This primary advantage can significantly assist in observing cracks in materials with complex microstructures such as nacre. In this direction, XFEM has been applied to predict the behavior of bone-inspired composites, showing good agreement between simulated and experimental crack propagation results [42,43]. The application of XFEM to nacre-inspired composites is not widely established [44]. Le, Ghazlan [44] created conch-inspired 3D-printed materials and validated their behavior with XFEM. They changed the printing nozzle path creating different material orientations that resemble aragonite distribution found on conch materials and evaluated the crack propagation with XFEM. The occurrence of mineral bridging was not studied.

Nacre mineral bridges (MBs) have recently been in the spotlight [30,45–49] because the mineral interconnections between rigid platelets can considerably increase the composite strength and toughness. Gu, Libonati [10] fabricated nacre-like composites through 3D-printing with different volume fractions of MBs, showing the influence of MBs on the material's mechanical properties. By solely increasing the MBs fraction, the strength of the composites directly rises. However, the toughness is increased only until a threshold and declines afterward. The influence of the MBs on the stress field was partially analyzed through finite element modeling and comparison with strain fields obtained from digital image correlation. Yet, crack propagation has not been numerically investigated. Askarnejad and Rahbar [47] showed that MBs and nanoasperities in the nacre platelets directly affect the material mechanical behavior. These nano-scaled features with near theoretical strength create a highly nonlinear material behavior. Moreover, the waviness of the platelets [48], and the organic matrix region in the proximity of MBs [49] can also influence the nacre behavior to exterior stresses.

In this work, bioinspired composites are modeled through XFEM to mimic the specific toughening mechanisms observed in nacre. The geometrical and material parameters followed previous studies [10,50,51], and additional experimental testing was carried out to support the data. Numerical analyses of tensile and fracture tests of brick-and-mortar composites were developed to observe the microstructural response to external loading, aiming at the fracture behavior. These models were divided into two main groups, (i) with and (ii) without mineral bridges (MBs), and categorized by their stiff component volume fraction: 50%, 60%, and 70%. Results showed that our XFEM models could predict experimental results with good agreement, especially for models without MBs. Moreover, the simulations showed that

MBs were able to arrest cracks, highlighting the MBs pivot role in increasing the material mechanical properties such as toughness and strength. Our work showed that an XFEM-based modeling approach can represent a useful framework for designing bioinspired composites with advanced microstructural features, such as the inclusion of material interconnections replicating MBs.

2. Material and methods

2.1. Materials design

Inspired by the brick-and-mortar structure (Fig. 1a), our composite design (Fig. 1b) is made of two constituents: VeroMagenta (VM) and TangoBlackPlus (TBP). VM represents the stiffer part of the composite, making up the aragonite phase in the natural counterpart. TBP is a soft-hyperelastic material, portraying the organic role played by nature. These materials were chosen as they can be together implemented into a multi-material commercial 3D printer (Objet500 Connex3, USA). Their material properties have been previously determined and described by Libonati and Gu [10,50,51]. To support the development of the hyperelastic model for TBP, a bi-axial tensile test was carried out. Numerical modeling of both the base materials and the composite materials was performed.

2.2. Experimental testing: bi-axial testing

Force-controlled biaxial tests were performed in a custom-made setup with appropriate specimen dimensions (Fig. 2) necessary due to the absence of bi-axial test standards [52]. The setup consists of four linear actuators that can apply independent displacements with sub-micron resolution (Fig. 2a and 2b). The test speed was 6 mm/min to reduce the viscoelastic effect found in rubber-like materials. The specimens have a cruciform geometry with slits in the arms to facilitate the load transfer (Fig. 2c and 2d). The local strain levels were measured by digital tracking marks added to the specimen surface. Bi-axial results were used as input to the simulations and can be seen in the Supporting Information (Fig. S1a).

2.3. Numerical modeling of base materials

The development of computational models replicating the uniaxial tests of single materials, VM and TBP, was the base to further create a more complex composite model. The XFEM is an extension of the conventional Finite Elements Method (FEM) and is used to solve fracture mechanics problems. The most convenient advantage of the XFEM is that the user does not necessarily need to set the crack initiation location. The method creates a crack when a few conditions are established, being the most disseminated when the local principal stress is higher than the material maximum principal stress (MAXPS). The crack propagation direction follows the damage evolution parameters. In our case, the crack is directed to a neighboring element from its start location when an element is under a local displacement higher than the threshold

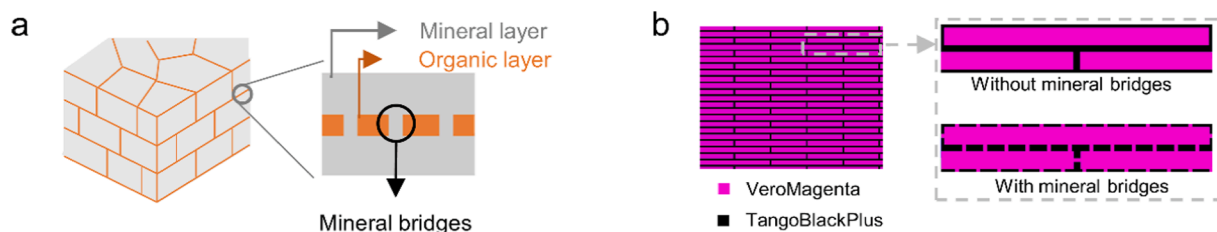


Fig. 1. (a) Nacre microstructure highlighting the aragonite mineral phase (in grey) and the biopolymeric organic layer (in orange), and the spatial locations of mineral bridges, connecting adjacent aragonite platelets across the biopolymer. (b) Overview of the bioinspired composite, made by 3D-printed materials: VeroMagenta (VM), mimicking the nacreous mineral phase, and TangoBlackPlus (TBP), as the biopolymeric organic layer. The composite has unit cells with or without bioinspired mineral bridges. (For interpretation of the references to colour in this figure legend, the reader is referred to the web version of this article.)

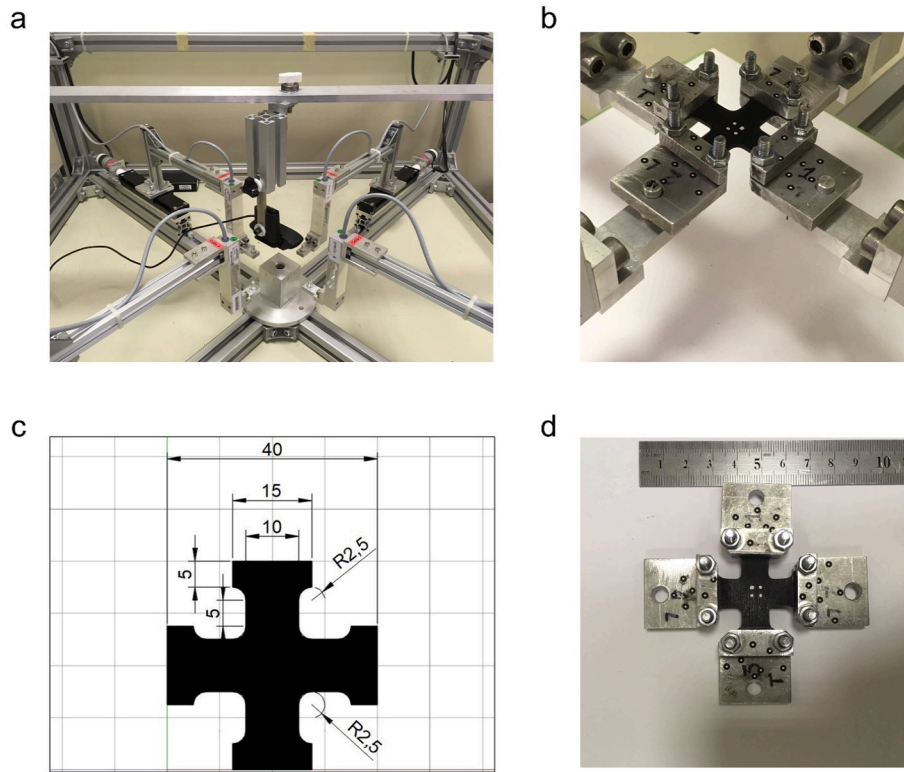


Fig. 2. (a) Bi-axial tensile test setup with (b) custom-made sample attached. (c) Dimensions of the specimen. (d) Overview of the clamped sample.

(e.g., maximum strain multiplied by the characteristic mesh element length). The procedure is repeated until the crack cannot propagate anymore, either due to a total failure or the non-achievement of local crack propagation conditions. Tensile and fracture tests were simulated using the software Abaqus 6.14.

- The 2D dog-bone tensile test geometry followed the experimental standard (Fig. S2a). The model was constrained in the left section and had a positive displacement in the right section while

constrained in the y-axis. The mesh comprehended 6528 CPS4R (linear quadrilateral plane stress with reduced integration) elements with coarse mesh in the extremities and more refined in the samples neck region, reached after a mesh sensitivity analysis (Fig. S2b and S2c).

- The fracture test geometry had a square-shaped configuration ($80 \times 80 \times 3$ mm), with a 16 mm lateral notch, represented in the simulation by a wire-type geometry (Fig. S3a). The model had a total of

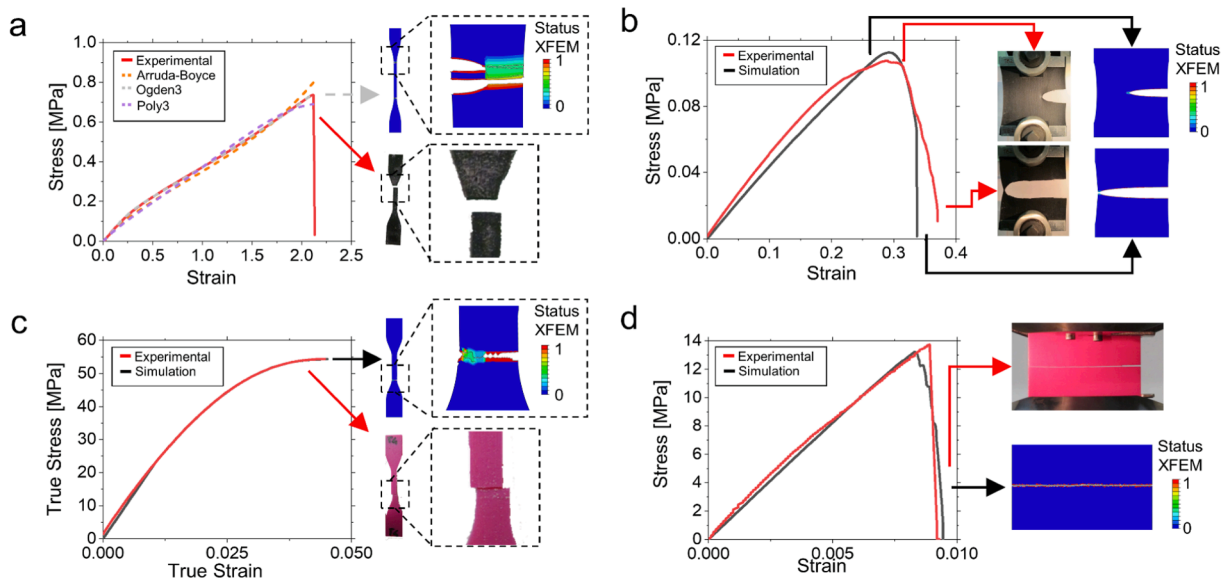


Fig. 3. (a) Comparison between the experimental and XFEM results for the (a, c) uniaxial tensile and (b, d) fracture test of (a, b) TangoBlackPlus and (c, d) Veromagenta. Status XFEM states the local crack propagation: being a full propagation the total element fracture is represented in red (Status XFEM = 1) and blue the opposite (Status XFEM = 0) [50]. (For interpretation of the references to colour in this figure legend, the reader is referred to the web version of this article.)

9100 CPS4R elements, obtained after a mesh sensitivity analysis (Fig. S3b and S3c).

The input VM material properties followed Libonati, Cipriano (42), (43) in both models. A biaxial tensile test was performed to obtain additional information for the hyperelastic material (*i.e.*, TBP), allowing a more accurate definition of the material model. The experimental results were compared to three numerical results run with different hyperelastic models: Arruda-Boyce, Ogden, and Polynomial. The Arruda-Boyce model [53] represents the material as a cubic element containing eight chains, with material-dependent three variables: μ , λ , and D . The Arruda-Boyce strain energy potential is $U = U(\mu_0, \mu, \lambda, D)$. However, at moderate strain, the accuracy of the model is not great [54]. The second-order polynomial model (Poly2) is based on the left Cauchy-Green deformation tensor, where $U = U(D_1, D_2, C_1, C_2, C_{10}, C_{11}, C_{20})$, but often overestimates the material properties [55]. The Ogden model is a model founded on the Helmholtz free energy. Its third-order strain energy is $U = U(\mu_1, \mu_2, \mu_3, \alpha_1, \alpha_2, \alpha_3, D_1, D_2, D_3)$. Despite having great accuracy, the model stability is very influenced by the input parameters [56]. The applied variables for the three models in the tensile test for single components are described in Table 1. In the fracture test simulations, the model adopted was Ogden3, followed by the results from the tensile tests.

2.4. Numerical models of nacre-like composite

The unit cells followed three configurations, with 50%, 60%, and 70% VM volume fractions. Detailed dimensions (Fig. S4a) are available in Table S1. Displacement conditions were applied to the two lateral edges, while symmetric boundary conditions were set to the others to replicate the presence of adjacent cells (Fig. S4b). The component material properties are shown in Table 2. The configuration has 13,850 four-node plane stress elements (CPS4R) with hourglass control. Hourglass control was adopted to overcome excessive distortion inherent to TBP material behavior. Mesh dependency analysis is shown in Fig. S4c. Analyses were run with a maximum number of cutbacks allowed for an increment (IA) of 20. The results of the numerical models were compared to experimental data available in a previous publication [10], where authors studied the influence of bridging in nacre-inspired composites varying the stiff volume fraction content (*i.e.* VM). The samples contained an edge crack in the design and were 3D printed using a multi-material printer (Objet500 Connex3, Stratasys). Experimental testing was performed under displacement-controlled tension in a universal testing machine at a 2 mm/min extension rate [10].

3. Results

3.1. Results for the homogeneous materials

For the TBP tensile test, computational results showed two cracks in mirrored positions in the region where the sample neck finishes. The cracks propagated equally, fracturing the specimen in two parts. Similar fracture behavior was described for the experimental result (Fig. 3a). The three hyperelastic models showed good agreement with the

experimental result in the uniaxial tensile test (Table 3). The Arruda-Boyce overestimated the strength by 8.4%, and the polynomial underestimated by 6.4%. The Poly2 model showed repeated convergence issues during computation, despite the small strength variation. Thus, the Ogden3 model was selected as the most adequate hyperelastic model for the TBP component.

Similarly, the fracture test replicated well the observed behavior, validating the choice for the Ogden3 hyperelastic material model (Fig. 3b). The crack propagated perpendicularly from the test displacement, growing horizontally until total fracture. The numerical analysis showed a material strength of 0.112 MPa and a strain at fracture of 33.7%, closely comparable to the experimental results of 0.107 MPa and 37.0%.

The tensile test results for VM showed the same failure mode as the experimental test: a crack started in the extremity of the sample neck region and led to the sample failure (Fig. 3c). The difference between the experimental and numerical material strength and stiffness was minimal, 0.02% and 3.45%, respectively (Table 4). For the fracture test, the crack continued from the predetermined initial location and propagated horizontally (Fig. 3d). The numerical maximum stress was 13.74 MPa, 3.9% higher than the experimental value (*i.e.*, 13.22 MPa). The failure modes of the tensile and fracture tests were identical to the reported experimentally (Fig. 3c and 3d).

3.2. Results for the bioinspired composites

The numerical models were evaluated according to their experimental counterparts. For the models without MBs, the accuracy varied with respect to the VM volume fraction (Table 5). The models with 50% and 60% had a high (*i.e.*, up to 48%) deviation from the experimental strength, determined as the maximum stress. On the contrary, the 70% model deviated only 0.68% from its experimentally measured strength value. For the toughness, calculated as the area underneath the stress-strain curve (until strain at rupture), the models were able to replicate the experimental behavior with a satisfactory accuracy (*i.e.*, between -8% to 9%). An increase in the VM fraction enhanced maximum strength but decreased strain at fracture, maintaining the toughness values within very similar ranges (Fig. 4a-c). Overall, the results showed that XFEM was able to predict the composite mechanical properties with reasonable accuracy. In the three models, the upper VM platelet arrested the crack tip, and an axial stress (S11) concentration at the tip was present (Fig. 5a). On the contrary, the lower platelets had higher shear stress (S12) and maximum absolute principal stress (MAXPS-AB) localized at the extremities furthest from the crack tip (Fig. 5b-c).

For the models with MBs, the quantitative comparison revealed high deviation for both strength and toughness (Table 6), in particular for models with a low VM volume fraction, such as the 50% VM-MB (Fig. 5f). Such models showed high stress concentration, which accentuates the occurrence of computational issues (*e.g.*, convergence issues and distorted elements), enlarging the gap between numerical and experimental results. The model with the stress-strain curve most similar to its experimental counterpart had the highest VM fraction (*i.e.*, 70%) (Fig. 4d).

Compared to their counterpart without MBs, all models with MBs

Table 1
Coefficients adopted for the hyperelastic models.

Model	Coefficients			
Arruda-Boyce	$\mu = 0.1373$	$\mu_0 = 0.1617$	$\lambda = 2.0821$	$D = 1.2370 \cdot 10^{-3}$
Ogden3	$\mu_1 = -52.2138$ $\alpha_1 = 1.0758$ $D_1 = 1.5097 \cdot 10^{-3}$	$\mu_2 = 26.0840$ $\alpha_2 = 1.2509$ $D_2 = 0.0000$	$\mu_3 = 26.2620$ $\alpha_3 = 0.8996$ $D_3 = 0.0000$	
Poly2	$D_1 = 0.2358$ $C_{10} = 0.8510$	$D_2 = 0.0000$ $C_{11} = 0.0288$	$C_1 = 0.0003$ $C_{20} = -0.0073$	$C_2 = -0.0110$

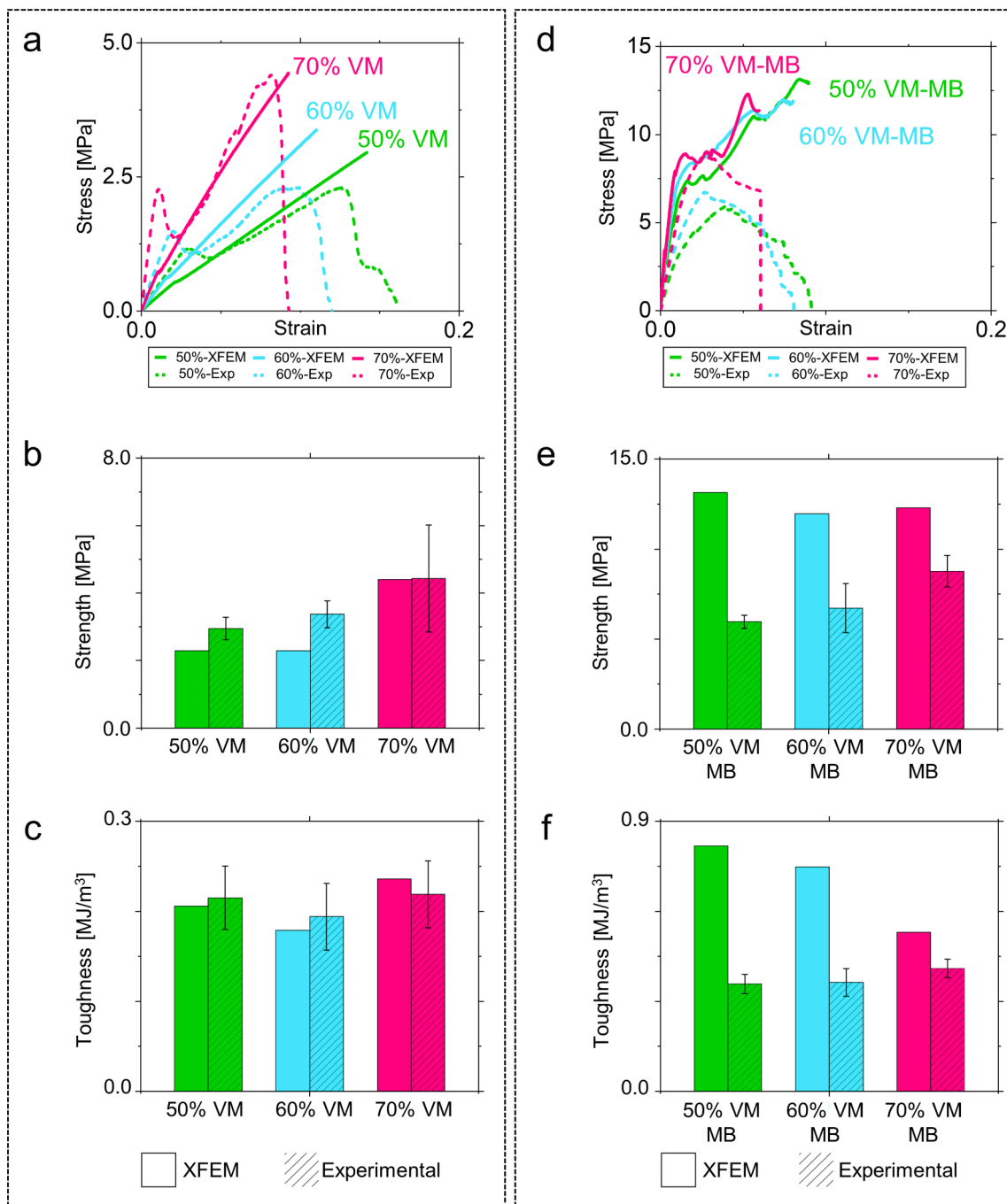


Fig. 4. Summarized comparison between the XFEM and experimental results for the models (a-c) without MBs and (d-f) with MBs. (a) Stress-strain curves. (b) Strength and (c) toughness bar plots.

Table 2
Material properties adopted to model TBP and VM.

Parameter	TBP	VM
Maximum principal stress	0.73 MPa	54.30 MPa
Displacement at fracture	0.5275 mm	0.0112 mm
Damage stabilization coefficient	$1 \cdot 10^{-6}$	$1 \cdot 10^{-4}$
Elastic modulus	–	2183.4 MPa
Hyperelastic model	Ogden 3	–
Poisson's ratio	0.49	0.35

Table 3
Strength comparison between the hyperelastic models and experimental for the TBP material under uniaxial tensile conditions.

Result	Strength [MPa]	Difference
Experimental	0.7373	–
Arruda-Boyce	0.7993	8.4%
Ogden3	0.7464	1.2%
Poly2	0.6902	–6.4%

Table 4
Strength comparison between the numerical and experimental for VM material under uniaxial tensile conditions.

Result	Strength [MPa]	Elastic modulus [MPa]
Experimental	54.37	2112.97
Numerical	54.36	2185.85
Difference	0.02%	3.45%

showed a stiffer behavior (Fig. 5g, h). Naturally, this is due to the platelet bridging, acting as an additional feature and enhancing stiffness during strained conditions. This is clear in all three samples, where the MBs in the middle sections have the highest compression stresses

Table 5
Evaluation of the numerical models without MBs.

Result	50% VM		60% VM		70% VM	
	Strength [MPa]	Toughness [MJ/m ³]	Strength [MPa]	Toughness [MJ/m ³]	Strength [MPa]	Toughness [MJ/m ³]
Experimental	2.29	0.206	2.29	0.179	4.4	0.236
Numerical	2.95	0.215	3.37	0.194	4.43	0.219
Difference	28.82%	4.36%	47.16%	8.37%	0.68%	-7.20%

(Fig. 5d). The strongest composite was the sample with 50% VM, but the variation compared to the 60% and 70% VM is low (Fig. 5h).

Regarding the shear stress response, for 50% and 60% VM, the highest absolute stresses are located in the MBs. Meanwhile, for 70% VM, they were in the VM platelets, more specific on the region in contact with the MBs (Fig. 5e). The stress fields are different for the maximum absolute principal stresses (MAXPS-AB) (Fig. 5f). The model with the lowest mineral fraction (i.e., 50%) has higher MAXPS-AB in the platelets. On the contrary, in the model with 70% VM, the MAXPS-AB peaks are in the mineral bridges. This change in stresses could be the reason for the material's lower toughness (Fig. 5g).

The crack propagation analyses reconfirm the role of the bridging

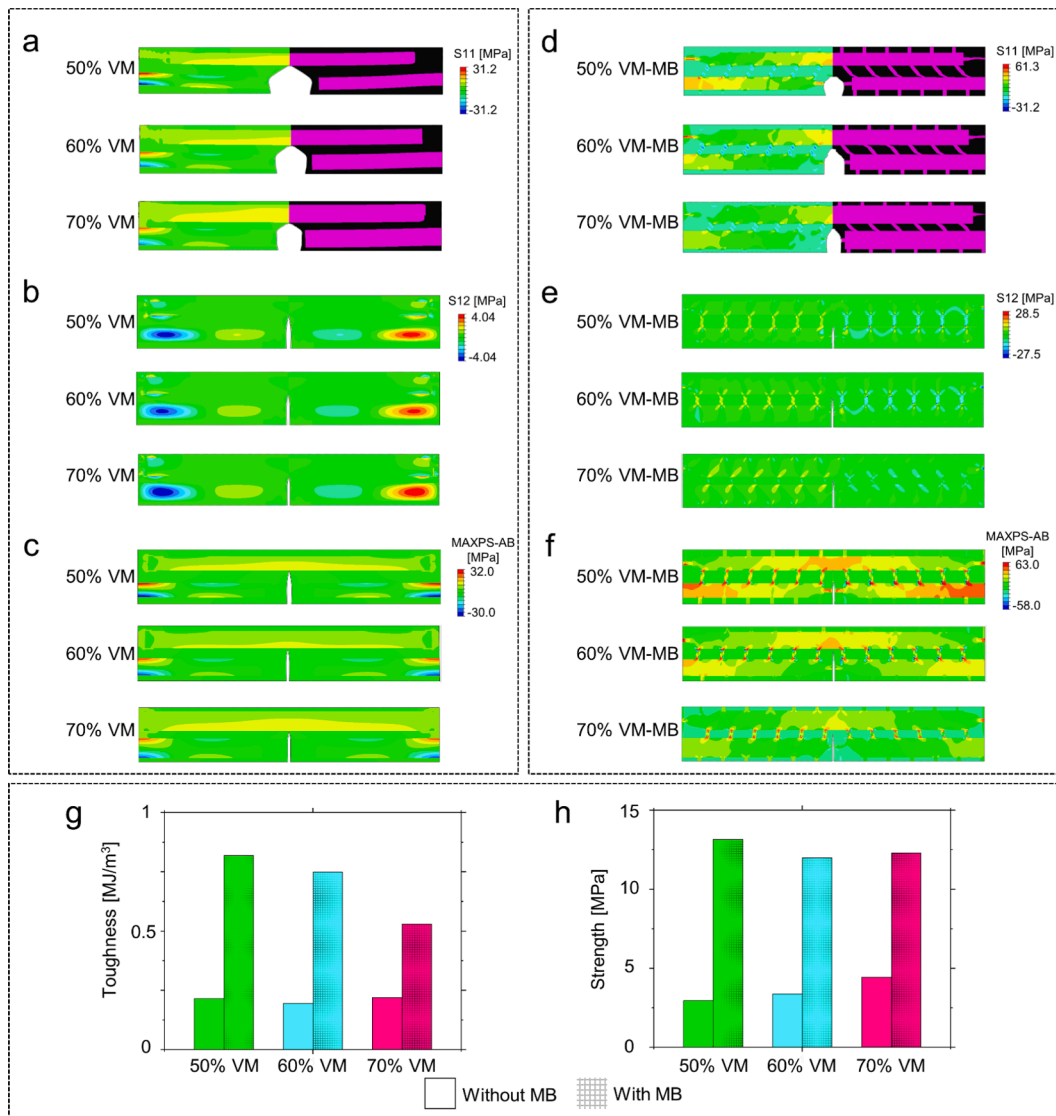


Fig. 5. Mechanical behavior of unit cells (a-c) without and (d-f) with MBs. Comparison between (g) toughness and (h) strength for the unit cells, showing that the inclusion of MBs enhances drastically the mechanical properties.

Table 6
Evaluation of the numerical models with MBs.

Result	50% VM-MB		60% VM-MB		70% VM-MB	
	Strength [MPa]	Toughness [MJ/m ³]	Strength [MPa]	Toughness [MJ/m ³]	Strength [MPa]	Toughness [MJ/m ³]
Experimental	5.96	0.358	6.72	0.363	8.77	0.41
Numerical	13.15	0.818	11.97	0.748	12.29	0.53
Difference	120.63%	128.49%	78.12%	106.06%	40.13%	29.26%

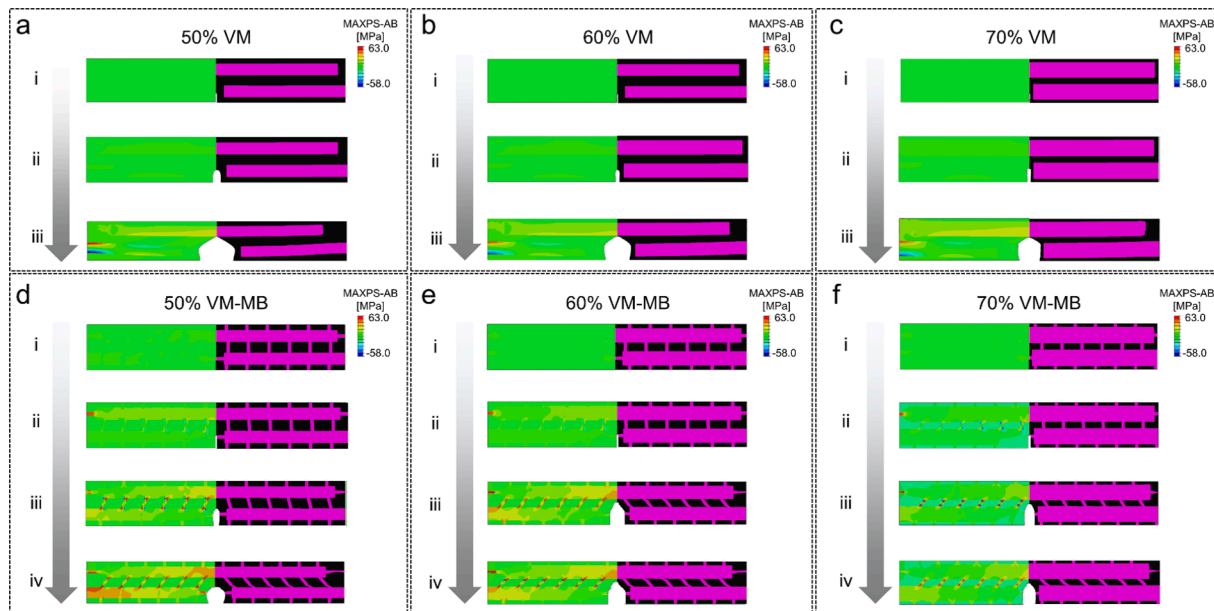


Fig. 6. Crack propagation for models with (a, d) 50% VM, (b, e) 60% VM, and (c, f) 70% VM, (a-c) without and (d-f) with mineral bridging. The maximum absolute principal stresses are shown for progressing steps (i-iv) for each configuration.

(Fig. 6). For all models with MB, between steps ii-iv, the stresses are intensified between the bridge/platelet regions (Fig. 6d-e), a clear contrast to their counterparts without MB (Fig. 6a-c).

4. Conclusions

In this work, we evaluated the application of XFEM as a method to simulate mechanical properties on a composite material with complex geometry and hyperelastic elements. By studying bioinspired nacreous designs with and without mineral bridging, we showed the capacity of XFEM to simulate failure in materials with hyperelastic behavior such as TBP. The support of previous works allowed a comparison with respect to the experimental results, validating the importance of mineral bridging on brick-and-mortar microstructures. Together with the toughness mechanisms of these structures, such as crack arresting on tougher platelets, our analyses found that bridging plays a significant role in the composite mechanical properties, especially because the MBs features act as sacrificial bonds, allowing energy release when the composite is bearing loads. The XFEM results showed higher strength and toughness for models with bridging compared to their opposite counterparts (e.g., without bridging). This trend is in agreement with the experimentally obtained results [10]. The influence of the additional platelet connection depends intensely on the dimensions of the bridges. In this work, the volume fraction of the stiffer element was chosen as a variable. For models without MBs, a higher volume fraction resulted in a much lower toughness, but insignificant strength alteration. Meanwhile, for the models with MBs, the increase in volume fraction raised the material strength without considerable variation of toughness. For models with MBs and low VM volume fraction, a larger gap between experimental and computational results was seen, possibly due to high

stress concentration that led to distorted elements and convergence issues. Our work showed that XFEM can be applied to simulate the failure of composite materials including a hyperelastic component with adequate accuracy and can be used as guidelines to design bioinspired composites that want to replicate mineral bridging.

Funding

This research did not receive any specific grant from funding agencies in the public, commercial, or not-for-profit sectors.

CRediT authorship contribution statement

Andres E. Aguilar Coello: Investigation, Methodology, Formal analysis, Software, Writing – original draft. **Andre E. Vellwock:** Formal analysis, Visualization, Writing – original draft. **Andrea Avanzini:** Investigation. **Flavia Libonati:** Conceptualization, Investigation, Writing – review & editing, Supervision.

Declaration of Competing Interest

The authors declare that they have no known competing financial interests or personal relationships that could have appeared to influence the work reported in this paper.

Data availability

Data will be made available on request.

Acknowledgements

The authors thank Laura Vergani and Pasquale Vena for insightful discussions.

Data availability statement

Data available on request.

Appendix A. Supplementary data

Supplementary data to this article can be found online at <https://doi.org/10.1016/j.compstruct.2023.117285>.

References

- [1] Vellwock AE, Yao H. Biomimetic and bioinspired surface topographies as a green strategy for combating biofouling: a review. *Bioinspir Biomim* 2021;16(4):041003.
- [2] Vellwock AE, Su P, Zhang Z, Feng D, Yao H. Reconciling the Conflict between Optical Transparency and Fouling Resistance with a Nanowrinkled Surface Inspired by Zebrafish's Cornea. *ACS Appl Mater Interfaces* 2022;14(6):7617–25.
- [3] Wei A, Yuan D, He B, Xie Y, Vellwock AE, Sun J, et al. Optimal Design for Higher Resistance to Thermal Impulse: A Lesson Learned from the Shells of Deep-Sea Hydrothermal-Vent Snails. *JOM* 2021;73(6):1714–22.
- [4] Johansson LC, Jakobsen L, Hedenström A. Flight in Ground Effect Dramatically Reduces Aerodynamic Costs in Bats. *Curr Biol*. 2018;28(21):3502-7.e4.
- [5] Jackson AP, Vincent JFV, Turner RM, Alexander RM. The mechanical design of nacre. *Proc R Soc B: Biol Sci* 1988;234(1277):415–40.
- [6] Song J, Fan C, Ma H, Liang L, Wei Y. Crack deflection occurs by constrained microcracking in nacre. *Acta Mechanica Sinica* 2018;34(1):143–50.
- [7] Barthelat F, Espinosa HD. An Experimental Investigation of Deformation and Fracture of Nacre-Mother of Pearl. *Exp Mech* 2007;47(3):311–24.
- [8] Grossman M, Bouville F, Masania K, Studart AR. Quantifying the role of mineral bridges on the fracture resistance of nacre-like composites. *Proc Natl Acad Sci USA* 2018;115(50):12698–703.
- [9] Checa AG, Cartwright JHE, Willinger M-G. Mineral bridges in nacre. *J Struct Biol* 2011;176(3):330–9.
- [10] Gu GX, Libonati F, Wettermark SD, Buehler MJ. Printing nature: Unraveling the role of nacre's mineral bridges. *J Mech Behav Biomed Mater* 2017;76:135–44.
- [11] Song F, Soh AK, Bai YL. Structural and mechanical properties of the organic matrix layers of nacre. *Biomaterials* 2003;24(20):3623–31.
- [12] Barthelat F, Tang H, Zavattieri PD, Li CM, Espinosa HD. On the mechanics of mother-of-pearl: A key feature in the material hierarchical structure. *J Mech Phys Solids* 2007;55(2):306–37.
- [13] Wang RZ, Suo Z, Evans AG, Yao N, Aksay IA. Deformation mechanisms in nacre. *J Mater Res* 2001;16(9):2485–93.
- [14] Gerhard EM, Wang W, Li C, Guo J, Ozbolat IT, Rahn KM, et al. Design strategies and applications of nacre-based biomaterials. *Acta Biomater* 2017;54:21–34.
- [15] Huang S, Phua SL, Liu W, Ding G, Lu X. Nacre-like composite films based on mussel-inspired 'glue' and nanoclay. *RSC Adv* 2014;4(3):1425–31.
- [16] Smith BL, Schäffer TE, Viani M, Thompson JB, Frederick NA, Kindt J, et al. Molecular mechanistic origin of the toughness of natural adhesives, fibres and composites. *Nature* 1999;399(6738):761–3.
- [17] Geng K, Xie W, Chen B, Yin Q, Yuan Y, Zhang Z. Failure simulation and design optimization of bioinspired heterogeneous interfaces by Floquet-based bar-spring model. *Compos Struct* 2020;252:112665.
- [18] Zhang Q, Li H, Liu Y, Zhang Z, Yuan Y. Nacre-inspired topological design tuning the impact resistant behaviors of composite plates. *Compos Struct* 2022;299:116077.
- [19] Greco F, Leonetti L, Pranno A, Rudykh S. Mechanical behavior of bio-inspired nacre-like composites: A hybrid multiscale modeling approach. *Compos Struct* 2020;233:111625.
- [20] Xiong D-B, Cao M, Guo Q, Tan Z, Fan G, Li Z, et al. Graphene-and-Copper Artificial Nacre Fabricated by a Preform Impregnation Process: Bioinspired Strategy for Strengthening-Toughening of Metal Matrix Composite. *ACS Nano* 2015;9(7):6934–43.
- [21] Wang S, Gao Y, Wei A, Xiao P, Liang Y, Lu W, et al. Asymmetric elastoplasticity of stacked graphene assembly actualizes programmable untethered soft robotics. *Nat Commun* 2020;11(1):4359.
- [22] Yin Z, Hannard F, Barthelat F. Impact-resistant nacre-like transparent materials. *Science* 2019;364(6447):1260–3.
- [23] Yourdkhani M, Pasini D, Barthelat F. Multiscale Mechanics and Optimization of Gastropod Shells. *J Bionic Eng* 2011;8(4):357–68.
- [24] Shao Y, Zhao H-P, Feng X-Q. On flaw tolerance of nacre: a theoretical study. *J R Soc Interface* 2014;11(92):20131016.
- [25] Bertoldi K, Bigoni D, Drugan WJ. Nacre: An orthotropic and bimodular elastic material. *Compos Sci Technol* 2008;68(6):1363–75.
- [26] Rudnitskyj A, Krenn S, Vorlaufer G, Gachot C. Influence of the 6061 Aluminium Alloy Thermo-Viscoplastic Behaviour on the Load-Area Relation of a Contact. *Materials* 2021;14(6):1352.
- [27] Rudnitskyj A, Larsson R, Gachot C. A Closer Look at the Contact Conditions of a Block-on-Flat Wear Experiment. *Lubricants* 2022;10(7).
- [28] Greco F, Leonetti L, Lonetti P, Nevone BP. Crack propagation analysis in composite materials by using moving mesh and multiscale techniques. *Comput Struct* 2015;153:201–16.
- [29] Xie W, Yuan Y, Zhang Z. A Floquet-Based Bar-Spring Model for the Dynamic Modulus of Bioinspired Composites With Arbitrary Staggered Architectures. *J Appl Mech* 2019;86(9).
- [30] Abid N, Mirkhalaf M, Barthelat F. Discrete-element modeling of nacre-like materials: Effects of random microstructures on strain localization and mechanical performance. *J Mech Phys Solids* 2018;112:385–402.
- [31] William Pro J, Kwei Lim R, Petzold LR, Utz M, Begley MR. GPU-based simulations of fracture in idealized brick and mortar composites. *J Mech Phys Solids* 2015;80:68–85.
- [32] Belytschko T, Black T. Elastic crack growth in finite elements with minimal remeshing. *Int J Numer Methods Eng* 1999;45(5):601–20.
- [33] Abdullah NA, Curiel-Sosa JL, Taylor ZA, Tafazzolmoghaddam B, Martinez Vicente JL, Zhang C. Transversal crack and delamination of laminates using XFEM. *Compos Struct* 2017;173:78–85.
- [34] Ahmad H, Crocombe AD, Smith PA. Strength prediction in CFRP woven laminate bolted single-lap joints under quasi-static loading using XFEM. *Compos Part A Appl Sci Manuf* 2014;66:82–93.
- [35] Benvenuti E, Orlando N, Ferretti D, Tralli A. A new 3D experimentally consistent XFEM to simulate delamination in FRP-reinforced concrete. *Compos B Eng* 2016;91:346–60.
- [36] Duarte APC, Díaz Sáez A, Silvestre N. Comparative study between XFEM and Hashin damage criterion applied to failure of composites. *Thin-Walled Struct* 2017;115:277–88.
- [37] Xie Y, Cao P, Liu J, Dong L. Influence of crack surface friction on crack initiation and propagation: A numerical investigation based on extended finite element method. *Comput Geotech* 2016;74:1–14.
- [38] Idkaidek A, Koric S, Jasiuk I. Fracture analysis of multi-osteon cortical bone using XFEM. *Comput Mech* 2017;1–14.
- [39] Rodriguez-Florez N, Carriero A, Shefelbine SJ. The use of XFEM to assess the influence of intra-cortical porosity on crack propagation. *Comput Methods Biomech Biomed Eng* 2017;20(4):385–92.
- [40] Gustafsson A, Khayyeri H, Wallin M, Isaksson H. An interface damage model that captures crack propagation at the microscale in cortical bone using XFEM. *J Mech Behav Biomed Mater* 2019;90:556–65.
- [41] Vellwock AE, Vergani L, Libonati F. A multiscale XFEM approach to investigate the fracture behavior of bio-inspired composite materials. *Compos B Eng* 2018;141:258–64.
- [42] Libonati F, Vellwock AE, Ielmini F, Abliz D, Ziegmann G, Vergani L. Bone-inspired enhanced fracture toughness of de novo fiber reinforced composites. *Sci Rep* 2019;9(1):3142.
- [43] Libonati F, Vellwock AE, El Louizi F, Hoffmann R, Colombo C, Ziegmann G, et al. Squeeze-winding: A new manufacturing route for biomimetic fiber-reinforced structures. *Compos Part A Appl Sci Manuf* 2020;132:105839.
- [44] Le TV, Ghazlan A, Ngo T, Nguyen T. Performance of a bio-mimetic 3D printed conch-like structure under quasi-static loading. *Compos Struct* 2020;246:112433.
- [45] Naglieri V, Gludovatz B, Tomsia AP, Ritchie RO. Developing strength and toughness in bio-inspired silicon carbide hybrid materials containing a compliant phase. *Acta Mater* 2015;98:141–51.
- [46] Le Ferrand H, Bouville F, Niebel TP, Studart AR. Magnetically assisted slip casting of bioinspired heterogeneous composites. *Nat Mater* 2015;14(11):1172–9.
- [47] Askarinejad S, Rahbar N. Toughening mechanisms in bioinspired multilayered materials. *J R Soc Interface* 2015;12(102):20140855.
- [48] Askarinejad S, Choshali HA, Flavin C, Rahbar N. Effects of tablet waviness on the mechanical response of architected multilayered materials: Modeling and experiment. *Compos Struct* 2018;195:118–25.
- [49] Askarinejad S, Shalchy F, Rahbar N. Role of interphase layers in mechanical properties of nacreous structures. *Compos B Eng* 2021;225:109255.
- [50] Libonati F, Cipriano V, Vergani L, Buehler MJ. Computational Framework to Predict Failure and Performance of Bone-Inspired Materials. *ACS Biomater Sci Eng* 2017;3(12):3236–43.
- [51] Libonati F, Gu GX, Qin Z, Vergani L, Buehler MJ. Bone-Inspired Materials by Design: Toughness Amplification Observed Using 3D Printing and Testing. *Adv Eng Mater* 2016;18(8):1354–63.
- [52] Avanzini A, Battini D. Integrated Experimental and Numerical Comparison of Different Approaches for Planar Biaxial Testing of a Hyperelastic Material. *Adv Mater Sci Eng* 2016;2016:6014129.
- [53] Arruda EM, Boyce MC. A three-dimensional constitutive model for the large stretch behavior of rubber elastic materials. *J Mech Phys Solids* 1993;41(2):389–412.
- [54] Chagnon G, Marckmann G, Verron E. A comparison of the physical model of Arruda-Boyce with the empirical Hart-Smith model and the Gent model. *Rubber Chem Technol* 2004;77.
- [55] Ju M, Jmal H, Dupuis R, Aubry E. A Comparison among Polynomial Model, Reduced Polynomial Model and Ogden Model for Polyurethane Foam. *Adv Mater Res* 2013;856:169–73.
- [56] Bergström J. Elasticity/Hyperelasticity. In: Bergström J, editor. *Mechanics of Solid Polymers*: William Andrew Publishing; 2015. p. 209–307.